





Resonant Auger spectroscopy on solid xenon on gold, silver, and copper substratesFredrik O. L. Johansson ^{1,2,3,*}, Elin Berggren ¹, Lucas M. Cornetta ^{1,4}, Denis Céolin,⁵ Mattis Fondell,⁶
Hans Ågren,¹ and Andreas Lindblad ¹¹Division of X-ray Photon Science, Department of Physics and Astronomy, Uppsala University, Box 516, SE-751 20 Uppsala, Sweden²Division of Applied Physical Chemistry, Department of Chemistry, KTH - Royal Institute of Technology, SE-100 44 Stockholm, Sweden³Sorbonne Université, CNRS, Institut des NanoSciences de Paris, INSP, F-75005, Paris, France⁴Department of Applied Physics, Gleb Wataghin Institute of Physics, State University of Campinas, Campinas, Brazil⁵Synchrotron SOLEIL, l'Orme des Merisiers, Saint-Aubin, Boîte Postale 48, 91192 Gif-sur-Yvette Cedex, France⁶Institute Methods and Instrumentation for Synchrotron Radiation Research PS-ISRR,

Helmholtz-Zentrum Berlin für Materialien und Energie, Albert-Einstein-Straße 15, 12489, Berlin, Germany



(Received 12 January 2023; accepted 14 February 2023; published 6 March 2023)

An investigation of the radiationless decay of core excited Xe atoms in the region of Xe $L_3M_{4,5}M_{4,5}$ Auger electron kinetic energies (using x-ray energies in the vicinity of the L_3 threshold) is presented for Xe adsorbed on Cu, Ag, and Au. The intensity distribution of the decay channels is different compared with Xe in the gas phase. Charge transfer of the core excited electron occurs within tens of attoseconds in all systems for excitation energies approaching the ionization threshold of the condensed system, whereas charge transfer times are substrate-dependent for lower excitation energies. The determination of partial yields into the decay channels allows for the observation of a decay channel present in the Xe/Cu and Xe/Ag systems but not in the case of Xe/Au. Theoretical calculations allow us to interpret this difference as emanating from varying amounts of the ground state hybridization between Xe and the substrates, which impacts the energy of the Auger final states enabling identification of these states giving rise to system specific features in the experimental data.

DOI: [10.1103/PhysRevA.107.032802](https://doi.org/10.1103/PhysRevA.107.032802)**I. INTRODUCTION**

The orbital character of unoccupied levels in an adsorbate system may be investigated through x-ray absorption spectroscopies (XAS) by detecting radiative (fluorescence) or nonradiative decays of a core excited metastable state [1]. In gas-phase systems, the nonradiative decay consists of a resonant Auger spectator at constant binding energy, and above the ionization potential, the normal Auger channel, at a constant kinetic energy, opens. In Fig. 1, x-ray core excitation and associated nonradiative Xe $L_3M_{4,5}M_{4,5}$ decay channels are schematically drawn. In the rightmost panel, the tunneling to a discrete set of bound levels—which may be occurring in the condensed phase—needs to be replaced with tunneling to a continuum for the gas phase. This process could then be thought of as a resonant shake-off of the core-excited electron accompanying the Auger decay [2–5].

In this paper, we study xenon adsorbed on gold, silver, and copper substrates. The initial excitation occurs from an atomic like core level of the adsorbate and can be expected to

remain similar to that of the gas phase, albeit shifted owing to interaction with the substrate. The system can thereby give a unique perspective on the substrate influence on the decay of excited states in an adsorbate as it can easily be compared to the gas phase. The inert nature of noble gases also provides insight into processes in single-atom physisorbed systems which can be compared to other adsorbates consisting of molecules that can be chemisorbed, physisorbed, or mixed where more processes compete. With a substrate the decay from the core-excited state now has an additional possible decay channel, the rightmost panel in Fig. 1. The electron in the core-excited state may tunnel away into a bound state elsewhere in the system from the site where the core-excitation occurred (see, e.g., Refs. [6–9]).

The most detailed study of the $L_3M_{4,5}M_{4,5}$ Auger spectrum of Xe in the gas phase is, to-date, by Kushawaha and coworkers resolving three contributions in the nd Rydberg series [10]. The selection rule quoted above indicates that $p \rightarrow s$ transitions are also present in dipole transitions. However, in the gas phase the intensity of the d -channel is fifteen times more intense than photoexcitation into the s channels [10]. Below we present results in the same kinetic energy range but for Xe adsorbed on three different coin metal substrates.

Watanabe measured XAS at the L_3 edge of Xe [11] and identified it as composed of $p \rightarrow s$ and $p \rightarrow d$ transitions using the mass absorption coefficient approach. Dezarnaud and coworkers included the calculations of the $2p \rightarrow nd$ Rydberg series leading to the $2p_{3/2}^{-1}$ ionization potential of gas phase Xe in total ion yield spectrum [12].

*fjson@kth.se

Published by the American Physical Society under the terms of the [Creative Commons Attribution 4.0 International](https://creativecommons.org/licenses/by/4.0/) license. Further distribution of this work must maintain attribution to the author(s) and the published article's title, journal citation, and DOI. Funded by [Bibsam](https://www.bibsam.org/).

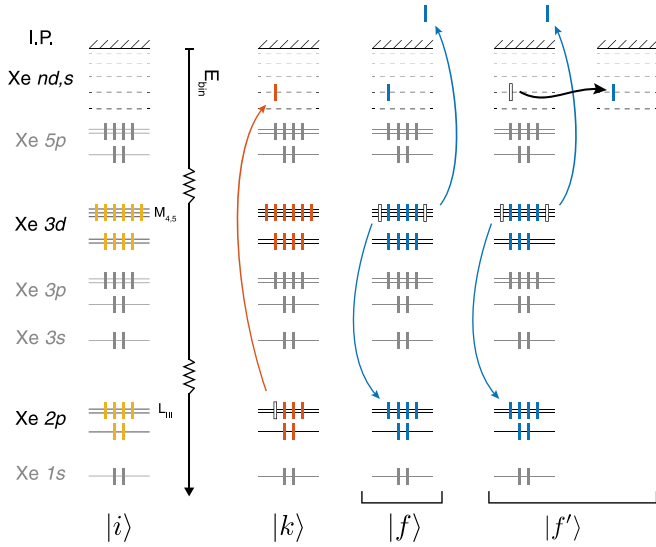
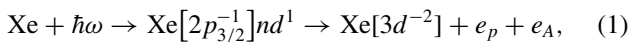


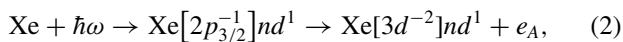
FIG. 1. Processes of core-excitation by an x ray and subsequent possible nonradiative decay routes of the intermediate core-excited state. The rightmost channel is possible in the condensed phase; in the gas phase the discrete state that the core-excited spectator electron tunnels into needs to be replaced by a continuum orbital—this electron participates in a shake-off process.

An alternative to measuring total yields is to measure the energy of the particles emanating from the system as a function of photon energy near the threshold. The decay yield of this metastable x-ray core excited state ($|k\rangle$) into various channels can be tracked with energy dispersive detection of, e.g., the radiative x-ray fluorescence channel [13] or the non-radiative (resonant) Auger channel [14]. The decay from the intermediate state, k , is governed by the Coulomb matrix element $I \propto \langle f | e^2 / r | k \rangle^2$. With an electron energy analyzer, the energies of resonant Auger spectator lines and normal Auger diagram lines were measured by Brown and co-workers [15] and used to decompose the L_3 absorption edge into components of the nd Rydberg series.

In gas phase Xe, two processes dominate in the nonradiative decay channel [14,15]. The Auger resonant double ionization process that gives rise to two electrons in the continuum via an intermediate state:

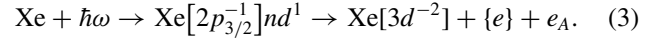


where the bracketed entity denotes orbitals with hole(s). Here the Auger electron e_A and a slow e_p photoelectron are emitted. This process gives rise to kinetic energies of the Auger electrons which are independent of the excitation energy. This may thus be dubbed an incoherent channel. Additionally, there is a possibility that the core excited electron remains in the nd orbital, screening an ionic core:



this is usually called a spectator Auger channel. The kinetic energy of the electron emanating from this process is $E_{\text{kin}} = \hbar\omega - E_B(3d^{-2}5d^1)$ if the spectator electron resides in the $5d$ orbital. The electrons observed from this process will thus have a constant binding energy—we call this the coherent channel which exhibits resonant Raman behavior [16,17].

In the condensed phase, the processes also involve screening from the substrate [17]. There is the possibility that the electron in the spectator orbital tunnels away from the core-excited site.



The curly brackets denote that the spectator electron has tunneled away from the core excited $\text{Xe}[2p_{3/2}^{-1}]nd^1$ state, leaving a $\text{Xe}[2p_{3/2}^{-1}]$ atom with the tunneled electron bound somewhere else in the system; the system can then decay by a process that is similar to a normal Auger decay, e.g., $\text{Xe}[2p_{3/2}^{-1}] \rightarrow \text{Xe}[2p_{3/2}] + \text{Xe}[3d^{-2}] + e_A$.

Close to the ionization threshold, process (1) can result in a photoelectron recapture owing to postcollision interaction (PCI) effect between the photoelectron and Auger electron in the continuum [18]. PCI without recapture result in a dependence on the excitation energy of the kinetic energy of both photo- and Auger electrons. It is still an incoherent channel since the initial energy of the Auger electron depends only on the orbitals involved in the Auger decay. For the Auger electron, PCI results in a blue shift of the kinetic energy since the slow photoelectron screens the doubly charged atom. In the condensed state, postcollision interaction is present if the screening of the ionic state is incomplete, as is the case for, e.g., free Xe clusters [19].

II. METHODS

A. Experiment

Experiments were performed using the high kinetic energy electron spectrometer (VG Scienta EW-R4000) located at the GALAXIES beamline, at the SOLEIL synchrotron (Paris, France) [20]. The undulator beamline is optimized for photon energies between 2.3 and 12 keV, and the photon polarization is horizontal and collinear with the spectrometer lens. x rays are energy-selected using a double crystal Si(111) monochromator. The experimental energy resolution was determined as 0.74 eV at 6000 eV photon energy by fitting the Au $4f$ lines which have a lifetime broadening of 0.3 and 0.28 eV for the $7/2$ and $5/2$ spin-orbit components, respectively [21]. Curve fitting of HAXPES and resonant Auger measurements were performed using the least-square fit method in the SPANCF [22,23] fitting procedure in Igor Pro. Errors were determined using the built-in error estimation procedure using Monte Carlo simulated data sets.

The base pressure in the analysis chamber was in the low 10^{-8} to high 10^{-9} mbar range. During the measurements, the photon beam was in grazing incidence with respect to the sample surface, meaning that the polarization vector is almost perpendicular to the sample surface. A closed cycle He-cryostat is installed on top of the solid sample 4-axis manipulator and allows reaching temperatures down to about 25 K close to the thermocouple. However attempts were made to adsorb argon on the metals at base temperature which was unsuccessful meaning that the temperature of the surface of the substrate was significantly higher than the thermocouple readout, probably 20–30 K above as argon was not adsorbing but xenon was.

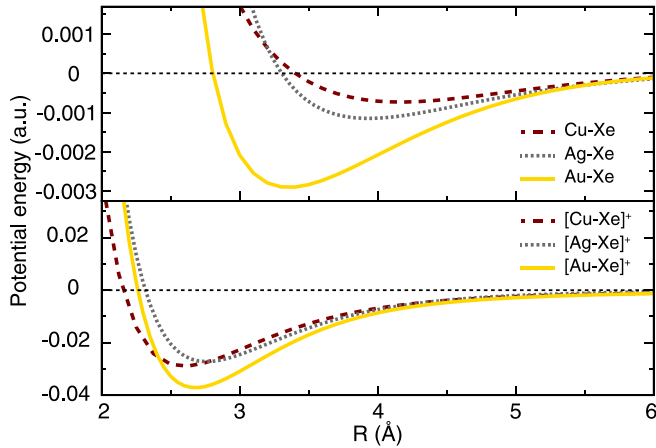


FIG. 2. Ground state potential energy curves, in atomic units, along the Au-Xe (yellow, solid line), Ag-Xe (gray, dotted line), and Cu-Xe (brown, dashed line) interatomic distances, in angstroms. The top graphics are the results for the neutral complexes and the bottom ones for the cationic systems.

Au foil (99.9%, MaTecK) was cleaned using 1 kV, 10 mA argon sputtering for 30 min at 2×10^{-6} mbar pressure, Xe was deposited at 3.5×10^{-7} mbar pressure for 4 minutes. Cu foil (99.99+%, MaTecK) was cleaned using repeated cycles of 2 kV, 10 mA argon sputtering at 3×10^{-6} mbar pressure. Xe was deposited at 2×10^{-7} mbar pressure for 5 minutes. Ag foil (99.99%, MaTecK) was cleaned using repeated cycles of 2 kV, 10 mA argon sputtering at 2×10^{-6} mbar pressure. Xe was deposited at 3×10^{-7} mbar pressure for 5 minutes. The Xe gas (99.999% Messer) was let into the analyzer chamber through a needle valve meaning that all depositions took place *in-situ* with the substrate cooled down to temperatures in the 30–40 K range according to the thermocouple readout. As discussed above, the actual temperature was higher than the thermocouple readout.

The bare metal surfaces were checked for oxide contribution using HAXPES prior to Xe deposition. The resonant Auger spectra were measured in resonant Raman conditions, meaning that the photon bandwidth is narrower than the lifetime of the core-excited state [24].

B. Theory

In order to investigate the influence of the substrates on the Raman and Auger states of Xe, theoretical studies were conducted considering the diatomic systems [Au-Xe], [Ag-Xe], and [Cu-Xe]. This minimalistic representation of a surface effect is called for because of the necessary combined correlated-relativistic treatment for the absorption. The ground state equilibrium geometries were characterized at the CCSD(T) level of theory. For the core-excited and ionized calculations the distances $R = 3.37$ Å for [Au-Xe], $R = 3.93$ Å for [Ag-Xe], and $R = 4.16$ Å for [Cu-Xe] were kept fixed. Further analysis of the potential energy scans indicate a significant shortening of the equilibrium distances upon ionization. The equilibrium distances of the cationic [Au-Xe]⁺, [Ag-Xe]⁺, and [Cu-Xe]⁺ species are, respectively, $R = 2.69$, 2.76, and 2.62 Å at the same level of theory (Fig. 2). The

fact that [Cu-Xe]⁺ equilibrium distance is slightly shorter than the [Au-Xe]⁺ one agrees with previous results [25]. Also in a good agreement with previous theoretical results is the relation between equilibrium distances of [Ag-Xe]⁺ and [Au-Xe]⁺.

The involved states—including the ground state, core-excited states $|2p_{3/2}^{-1}6s^1\rangle$, $|2p_{3/2}^{-1}5d^1\rangle$ and $|2p_{3/2}^{-1}6p^1\rangle$, core-ionized states $|2p_{3/2}^{-1}\rangle$, Raman and Auger states—were characterized with RASSCF/RASPT2 calculations, as implemented in the OpenMolcas program [26], together with the ANO-RCC-VQZP basis set. Relativistic effects were included considering the Douglas-Kroll transformation of the Hamiltonian and spin-orbit couplings were included by the RAS variational State Interaction procedure. The initial reference for all calculations was represented by the restricted Hartree-Fock orbitals obtained for the closed shell anionic [Au-Xe]⁻, [Ag-Xe]⁻, and [Cu-Xe]⁻ systems. For the core-excited and core-ionized states, the active space was designed considering the balance of natural occupation numbers, the lowering of total energy, on tests that main interactions are included, and a consideration of computational cost. The finally chosen active space comprises the three Xe $2p$ orbitals, the occupied valence orbitals of the metal atoms, and the $6s$, all $6p$ and all $5d$ virtual orbitals of Xe. That results in 17 electrons in 18 orbitals for the excited states and 16 electrons in 18 orbitals for the ionized states for all three systems, where RAS1/RAS2/RAS3 restrictions were imposed accordingly.

Calculations of the excited states for pure gas phase Xe were also performed in order to get insight about the substrate effects. In that case, the active space contemplates the three Xe $2p$ orbitals, and the $6s$, all $6p$, and all $5d$ virtual orbitals of Xe, resulting in 6 electrons in 12 orbitals. In order to obtain the electric dipole forbidden transitions $|2p_{3/2}^{-1}6p^1\rangle$, electric quadrupole and magnetic dipole moments were included in the total transition strengths. All absorption spectra are shown in Fig. 3.

For the ionized state we obtained 4797.53 eV as the ionization potential of [Au-Xe], 4798.03 eV of [Ag-Xe], and 4798.14 eV of [Cu-Xe]. All the results differ from the experimental value by less than 0.2%—the discrepancy is mainly due to higher order relativistic effects that are not included at this level of theory.

In addition, the Xe[$3d^{-2}$] doubly ionized states corresponding to the resonant Auger process were also characterized within the same methodology. In these cases, the active space comprises the five Xe $3d$ orbitals (RAS1) and the occupied valence orbitals of the metal atoms (RAS2). That results in 21 electrons in 11 orbitals for the ground state and 19 electrons in 11 orbitals for the doubly ionized states for all three systems. The results are presented and discussed in Sec. III B.

III. RESULTS AND DISCUSSION

A. Core-level spectra and coverage

In Fig. 4(a), we present the Xe $2p_{3/2}$ core-levels recorded at 6000 eV photon energy on all substrates. The binding energies are found at 4778.42 ± 0.02 , 4779.12 ± 0.02 , and 4779.41 ± 0.02 eV for Au, Ag, and Cu, respectively, and can

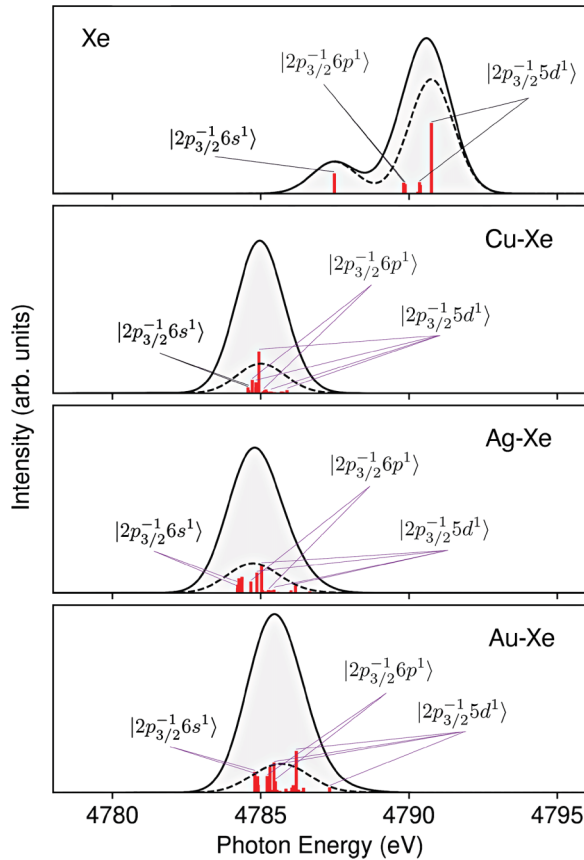


FIG. 3. Theoretical absorption spectra of pure Xe, [Cu-Xe], [Ag-Xe], and [Au-Xe] systems. The graphics were shifted by the respective error values obtained for the $2p$ ionization potentials. The most significant transitions dominated by the relevant single excitations are indicated. For comparison, the absorption spectra obtained only within the electric dipole approximation is also shown (dashed lines).

be compared to the gas phase binding energy of 4786.3 [27] or 4787.3 eV [28]. There is a clear shift of 0.98 eV between Cu and Au, with the Cu substrate giving the higher binding energy. The difference in work function of a Xe film on Cu versus Au is 0.87 eV and the difference in surface potential is 0.04 eV which is close to the binding energy difference. For Ag versus Cu, the binding energy difference is 0.29 eV with a work function difference of -0.01 eV and a surface potential difference of 0.20 eV [29].

The coverage of Xe is estimated by measuring the Xe $4d$ core level, as shown in Fig. 4(b) for the Cu case. The corresponding binding energies of the $5/2$ and $3/2$ components are 62.94 ± 0.01 and 60.97 ± 0.01 eV, respectively, which is close to the value found by Bendouan for a monolayer coverage on Cu(111) (63.04 and 61.07 eV) whereas a bilayer coverage will show an additional peak at approximately 0.5 eV higher binding energy [30]. The adsorption of Xe monolayers can be done at temperatures around 60–65 K at a pressures of 10^{-6} mbar [31] and the phase diagram of Xe adsorption on Ag [32] shows that for temperature in the 60 K range monolayer coverage is stable up to high gas pressures before bilayer formation. Similar behavior, with monolayer formation at these temperatures have also been seen on Au

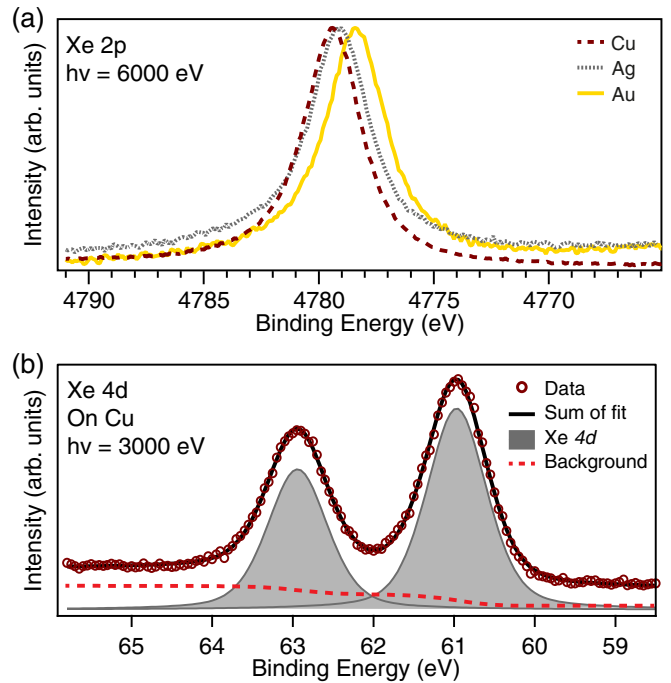


FIG. 4. (a) Xe $2p_{3/2}$ HAXPES spectra on the three substrates and (b) the Xe $4d$ photoelectron spectrum together with a least squares fit on Cu.

substrates [33]. Considering the Xe $4d$ peak positions and the temperature range where the deposition was performed we can conclude that the Xe coverage is monolayer.

On the Au foil substrate, the Xe $4d$ lines coincide with the gold lines making an accurate fit of the lines more difficult. However, we extracted a binding energy for the Xe $4d_{5/2}$ of 60.95 eV. The Xe $4d$ spectra were not recorded for the Ag sample.

B. Theoretical results

Comparing the calculated XAS spectra from Fig. 3 with the experimental Xe high-energy resolution off-resonant spectroscopy (HEROS) $2p_{3/2}$ XAS spectrum indicates an almost perfect match. The HEROS spectrum is derived in Ref. [34] from the resonant inelastic x-ray scattering spectrum and corresponds to an absorption signature with a spectral resolution defined only by the very narrow final-state broadening. The relative intensities and energies of the $6s$ and $5d$ transitions are well described. Also, the $6d$ transitions—not included in our calculations—are predicted to situate very closely above the $5d$. In the spectrum, an additional peak at 4785.5 eV is here interpreted as the onset of the ionization potential. Note that we used an *ad hoc* narrow line broadening, much narrower than the true width, about ten eV broad in the photoelectron spectrum, see Fig. 3, concealing all structures in the true absorption spectrum [34]. Our calculations show that, although the inclusion of electric quadrupole transitions are relevant for describing $|2p_{3/2}^{-1}6p^1\rangle$ states, they contribute only marginally to the dipole-dominated $6s$ and $5d$ transitions.

The comparison between the solid and dashed lines in Fig. 3 shows the deficiency of the electric dipole

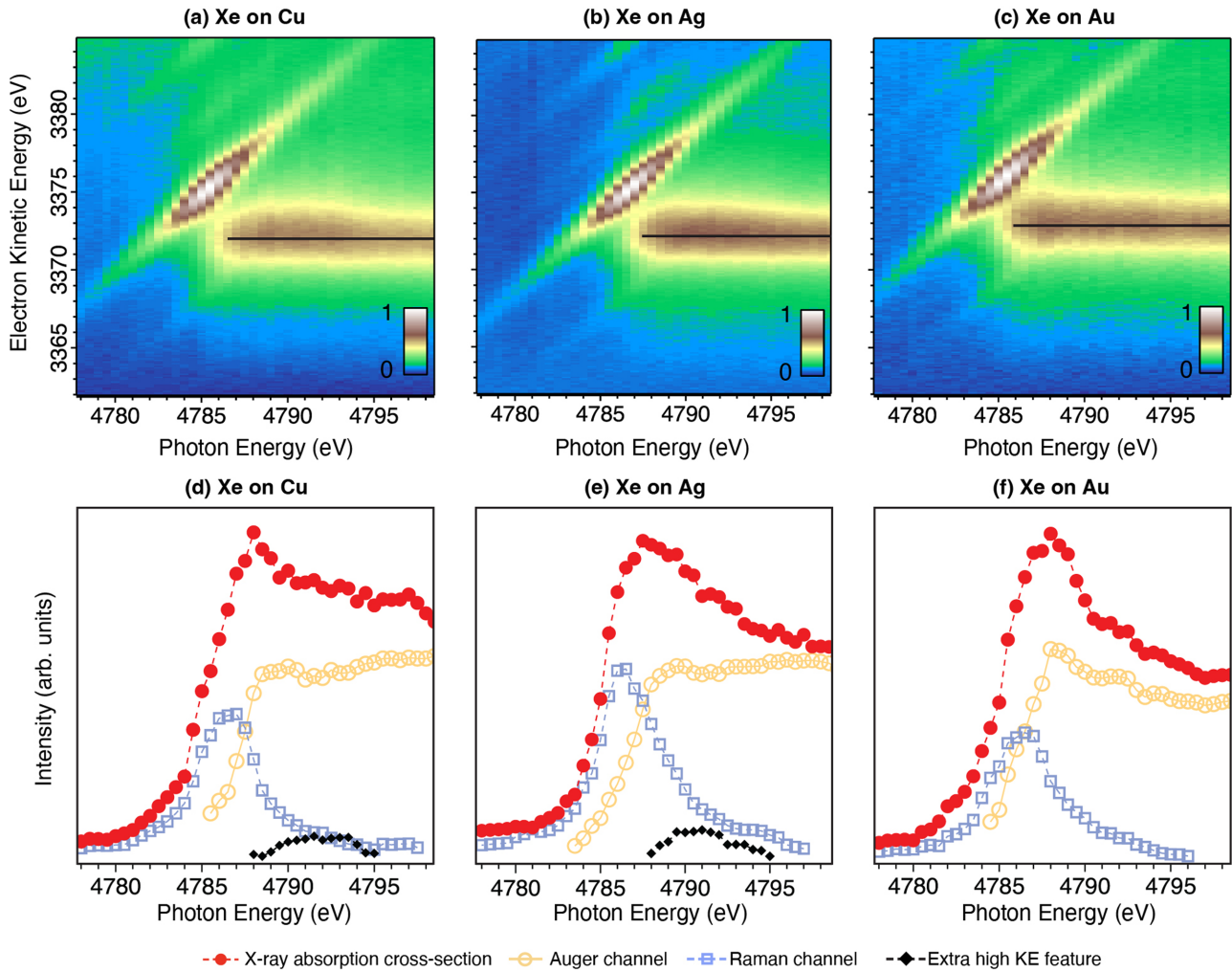


FIG. 5. (Top) Maps of the electron kinetic energy distributions measured in the range of Xe $L_3M_{4,5}M_{4,5}$ Auger electrons upon x-ray excitation scanned over the Xe L_3 edge on (a) Cu, (b) Ag, and (c) Au. The solid line through the maps highlight the asymmetry on the Auger channel formed by the extra high kinetic energy feature described in the text. (Bottom) x ray absorption cross sections obtained from the row-wise intensity sum of the 2D-maps with partial yields created from a least squares fit to the electron spectra on (d) Cu, (e) Ag, and (f) Au.

approximation for the adsorbed Xe, in contrast of pure Xe. In the minimalistic model we use the atomic symmetry lost imposed by the metal atoms allows quadrupole transitions that were forbidden in gas phase. Besides, the addition of a surface atom introduces an overall down shift on the absorption bands (5 to 7 eV for the three cases) and a grouping of the main $6s$, $5d$, and $6p$ pure Xe transitions, leading to a variation of the total spectral shape. The modification owes to the hybridization bond upon optical excitation. We can observe that the structures become broader according to the sequence Cu, Ag, Au, in which it is notable that the [Au-Xe] absorption differs more significantly from the other two in that sense. This can be compared to the experimental measurements. In the x-ray absorption presented in Fig. 5 (bottom), the features corresponding to the Raman channels (constant binding energy) are expected to be somehow proportional to the excitation signature. For the Au case we can observe a slightly broader structure, in comparison to the Cu and Ag cases, which agrees with the theoretical results. In view of the agreement, we therefore understand that the $|2p_{3/2}^{-1}6s^1\rangle$ and $|2p_{3/2}^{-1}6p^1\rangle$ states significantly contribute to the excitation profile.

As discussed below, for comparative adsorbate systems, a bond with π symmetry along the surface normal may be created from hybridization of the $6p5d$ valence orbitals [35,36]. This thus seems to be the case also for the systems studied here.

The analysis of the charge density associated with the ground and excited states is a good ground for investigating the hybridization and charge transfer features. In the ground states, the Xe partial atomic charge is +0.01 for [Cu-Xe], +0.01 for [Ag-Xe], and +0.12 for [Au-Xe]. The population of the metal atoms is still quite marginal indicating the physisorbed (dispersion) nature of the ground state bonding, although we see a little more mixture for [Au-Xe]. In this latter case, we assign the stronger covalent nature of the bond mainly as a consequence of the short interatomic distance. For the core-excited states, we looked at the Xe atomic charges for all states considered in the absorption spectra displayed in Fig. 3. The histograms in Fig. 6 show how the charge is transferred into the metal in all three cases. We can see that for [Cu-Xe] and [Ag-Xe] the Xe atomic charge remains close to zero in the major part of the excited states. However, for

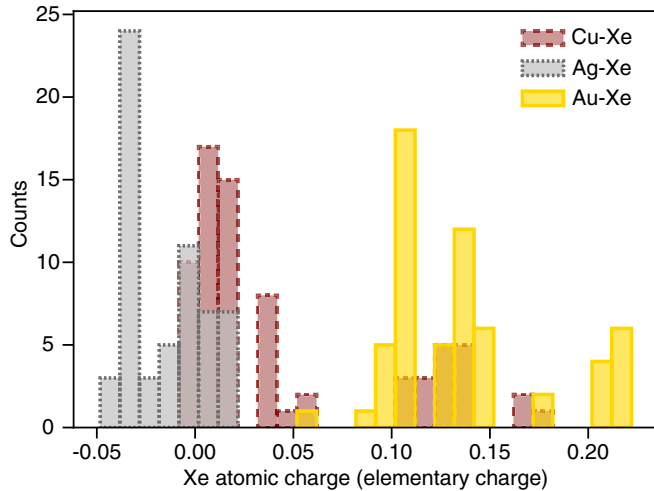


FIG. 6. Histograms of the distribution of Xe atomic charges over all excited states considered for the calculation of the absorption spectra shown in Fig. 3.

the [Au-Xe] case, we observe a partial charge transfer from Xe to Au—from 0.05 to 0.23 units of elementary charge, which supports the idea that the higher hybridization in the [Au-Xe] ground state correlates to a higher charge transfer in the excited states, in comparison to the Cu and Ag cases. The charge transfer tendencies obtained by the minimalistic model may be qualified by the fact that even in a semi-infinite representation of the metal any charge deposited from the Xe atom will be strongly bound to the connecting metal atom owing to the strong Coulombic attraction of the Xe $2p$ core hole.

For the doubly-ionized Auger states, we calculated the energies of the lowest-lying Xe[$3d^{-2}$] as being 1414.56 eV for Cu-Xe, 1416.79 eV for Ag-Xe, and 1413.19 eV for Au-Xe, all in relation to their respective neutral ground states. We observe that there is a good match when comparing these values with the Auger channels in the measurements of the coincidence (Fig. 5). In fact, the onset of the horizontal features in the 2D maps correspond to Auger states around 1415 eV for Cu-Xe and Ag-Xe, while for Au-Xe, this is about 1 to 2 eV below.

C. Resonant Auger in the $L_3M_{4,5}M_{4,5}$ region

Auger spectra in the $L_3M_{4,5}M_{4,5}$ kinetic energy region were recorded while stepping the photon energy over the L_3 ionization edge [Figs. 5(a)–5(c)]. The corresponding 2D maps are normalized to the maximum intensity on the low kinetic energy side of the spectra. Several decay channels are visible, the strongest one being the dispersing spectator channel attributed to the $3d^{-2}5d^1$ final state. Above the ionization threshold the horizontal line corresponds to the normal Auger channel. However, contrary to the gas phase case, it does not exhibit a strong PCI shift towards higher kinetic energies.

Compared with previously published gas phase spectra [10] only one additional spectator state is visible very close to the onset of the normal Auger line is present in the solid case, and is attributed to the $[3d^{-2}]6d$ final state. In contrast to the Raman line of the $[3d^{-2}]5d$ final state, the other Raman

features terminate when the Auger channel is open. For the $L_3M_{4,5}M_{4,5}$ of Cu and Ni, the resonant Raman features disperse until the normal Auger channel is open and coherence is lost [37,38]. In our case, we thus observe no loss of coherence for the $5d$ excited state, but $nd > 5$ behave differently as their intensity dissipates when the normal Auger channel opens.

The kinetic energy difference between these Raman features are 6.2 eV for Au and Cu and 6.1 eV for Ag in our data that can be compared to 6 eV reported in the gas phase [10]. The yield of the channels $nd > 5$ is small compared to the gas phase.

Excitations into the ns levels would appear at higher excitation energy but are not seen in neither sample due to their very weak coupling with the $2p$ orbitals. In the gas phase, the intensity of these lines are 15 times lower than that of the $2p \rightarrow nd$ transitions [10].

Above the threshold, there is a noticeable difference between the three substrates. In the case of Au the normal Auger spectra has constant kinetic energy position and width. In the case of Cu and Ag, however, looking at the intensity of the Auger channel above the solid black line there is a seemingly extra intensity appearing on the high kinetic energy side between 4787 and 4794 eV. This contribution is extracted and shown in Figs. 5(e) and 5(f).

D. Partial yields

The partial Auger electron yields (PAY) and partial Raman yields (PRY) extracted from the areas of incoherent Auger-like decays and coherent Raman-like decays are presented in Figs. 5(d)–5(f). Areas were obtained from a fit with a Shirley type background [39] and the Auger peaks were modeled using Voigt line shapes. To model the full background shape, the Shirley type background needs to be augmented with an extra intensity which we model using a very broad Gaussian contribution for all spectra, this behavior is the same on all substrates albeit with varying widths and intensity of the Gaussian. For Ag and Cu, the Gaussian is 20% and 6% of the height of the CT Auger channel respectively and width slightly above 5 eV FWHM. In the case of Au it is again 20% of the Auger channel height but with 3.2 eV FWHM. This augmentation of the background is not a new physical feature, a broader kinetic energy window would allow the Shirley integration to converge to a shape akin to that of the background we used here.

The x-ray absorption cross-section measured as a partial electron yield (PEY, here obtained from the row-wise sum of intensities in the kinetic energy region studied) is shown in Figs. 5(c) and 5(d). The partial Auger and Raman yields (PAY and PRY) are the areas calculated from the spectral fits of the respective channel. The two yields highlight two different regions of the x ray absorption PEY spectra. The first resonance arises from the most intense Raman channel belonging to the $[2p_{3/2}^{-1}]5d$ state. At a certain energy near threshold, the PAY and PRY cross each other after which the normal Auger channel takes over most of the intensity.

Partial yields extracted from the gas phase data from reference [14] exhibit the same behavior, albeit with the $5d$ and $nd > 5$ yields well separated.

Additional high kinetic energy parts of the normal Auger spectrum may arise from lowering of the Coulomb repulsion between holes in the final state (e.g., Ref. [40]). One may argue that this might arise from Xe atoms in a second layer, whose chemical shift in normal Auger would reside in the vicinity of those we observe [41]. In both these, cases we would observe persisting features either in the normal Auger spectrum or in the core-level photoelectron spectrum.

Sandell *et al.* have studied core excitation of argon atoms on various metallic substrates together with experiments on argon codeposited with potassium [42]. The core excitation of Ar $2p_{3/2} \rightarrow 4s$ creates a state similar to that of the potassium ground state [43]. Analogously we would look for the $Z + 1$ in relation to Xe: cesium. Furthermore, inverse photoemission studies of Xe monolayers on Ru(001) populate $6s$ and $6p5d$ levels [44] akin to those populated in the ground state of Cs.

For Cs at Cu (and other alkali metals/noble metal combinations), there exists the possibility of creating a hybridization bond upon optical excitation. For Cs/Cu(111), a bond with π symmetry along the surface normal may be created from hybridization of $6p$ - $5d$ valence orbitals—as described by Borisov and coworkers who have investigated this state with both theoretical and experimental methods [35].

As shown above, our calculations (and others [25]) show that the ionic state $[\text{Cu} - \text{Xe}]^+$ has a shorter bond length than $[\text{Au}-\text{Xe}]^+$, which is a possible explanation for the observed extra intensity in the case of Cu but not in Au—the overlap in the hybridization between substrate and adsorbate orbitals must necessarily depend on the distance between the involved atoms. However, this is invalidated by $[\text{Ag}-\text{Xe}]^+$, where extra intensity is present even though the bond length is longer than that of $[\text{Au}-\text{Xe}]^+$.

The extra feature can be explained from the efficiency in charge transfer. As explained above, the $[\text{Au}-\text{Xe}]$ system maintains a swift charge transfer as compared to the other cases where the transferred electron stays closer to the excitation site in the case of both $[\text{Ag}-\text{Xe}]$ and $[\text{Cu}-\text{Xe}]$. The presence of the electron that tunnels away but remains close, thereby partly screening the ionization site, gives the emitted Auger electron a slightly higher kinetic energy. This is also observed upon complete charge transfer from the surface to an adsorbate, as shown for C_{60} on Au [45].

E. Postcollision interaction

Postcollision interaction between the Auger electron and the photoelectron in the continuum—particularly close to threshold—gives rise to a continuous blueshift of the Auger electron away from the diagram Auger line and correspondingly a redshift of the photoelectron. In a classical description, a slow photoelectron sees a singly charged ion until the fast Auger electron overtakes it. At that point, the photoelectron is suddenly exposed to a electrostatic potential of a doubly charged ionic core leading to a loss of velocity, whereas the Auger electron is accelerated due to a rapid change of the central potential from a $+2$ to a $+1$ charge. This occurs at a point away from the ion that depends on the relative velocities involved, hence a dependence on the excess energy driven by the excitation energy would be expected. Sufficiently far

above threshold, a semiclassical approach describes the process well [18]. This can be seen in Ref. [10] where the shift away from the nominal Auger line diminishes upon increasing photon energy. Closer to threshold the shifts are larger and intertwined with a possible recapture processes of the slow electron into Rydberg states. In this case a quantum mechanical picture is necessary for a proper description [46–48].

In Fig. 5, we do not observe a clear shift away from the constant kinetic energy progression for the Auger channel, in the photon energy window under investigation. The shifts in intensity close to threshold emanates from faint Raman channels with $nd > 5$. If the screening was incomplete, or belonged to the surrounding Xe neighbors, a PCI-shift would be present, albeit damped [19]. PCI gets suppressed when there is no dicationic state to switch on/off, i.e., in the case of complete screening. For Cu-clusters this is an emergent effect and, at a certain size, the cluster's electronic properties turn metallic and the PCI of Auger and core-levels disappear [49]. This is valid in the present case for all substrates where no strong PCI shift can be observed, meaning that the final states are completely screened by substrate effects.

F. Core-hole clock

Looking back at Fig. 1, we can see that we have determined the partial yields in the coherent Raman channel and the incoherent Auger-like channel. The former constitutes a process that remains local at the site of core excitation whereas the other involves processes that see the core excited electron tunnel away from the site of excitation. The relative propensity for those channels can be used together with the lifetime of the excited state τ to determine the time within which the electron has tunneled away. At resonance, the lifetime of the core-excited state is the lifetime of the core-hole, as derived from $\tau = \hbar/\Gamma_L$. Γ_L is the lifetime width of the core-hole determined from the Lorentzian component of the signature in the photoelectron spectrum and \hbar is the reduced Planck constant. However, detuning off the resonance the lifetime of the excited state also contains a scattering component [50], this total time we refer to as the duration timed of the resonant scattering process, τ_c and can be calculated as

$$\tau_c = \frac{\hbar}{\sqrt{\Omega^2 + \Gamma_L^2}}, \quad (4)$$

where Ω is the detuning relative to the characteristic energy of the x-ray absorption band, here taken as the maximum intensity of the Raman feature. The charge transfer time (τ_{CT}) can then be calculated as

$$\tau_{\text{CT}} = \frac{I_{\text{Raman}}}{I_{\text{Auger}}} \tau_c. \quad (5)$$

The core-hole lifetime of Xe $2p_{3/2}$ core-hole was determined through a least squares fit to the HAXPES spectrum in Fig. 4 using a Voigt function. Using the Gaussian part (0.74 eV and 0.72) determined from Au $4f$, as mentioned above, to represent the experimental broadening, we get the core-hole lifetime from the Lorentzian lifetime broadening Γ_{L_3} of 2.79 ± 0.02 eV (which is within 2% of the tabulated

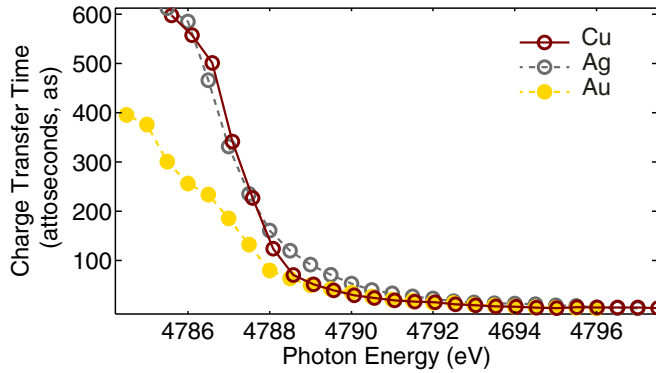


FIG. 7. Charge transfer times calculated from Eq. (5) for [Cu-Xe], [Ag-Xe], and [Au-Xe]. Propagated errors in the charge transfer time lie within the size of the marker.

value [51,52]). The core-hole lifetime determined from the Heisenberg uncertainty relation $\tau_{2p_{3/2}} = \hbar/\Gamma_L$ is then 236 ± 1 as.

Looking qualitatively on the derived charge transfer times in Fig. 7(c), the charge transfer time for [Au-Xe] is clearly faster than the other substrates in the region close to absorption maximum. This is in concurrence with our theoretical results as explained above. The charge transfer times can be divided into two regions with distinctly different behavior: one where the charge transfer time varies rapidly with the excitation energy below threshold (located at about 4786 eV photon energy) and one that varies slowly with the excitation energy above threshold. Looking in Fig. 5 we see that both partial Raman and Auger yields increase up to a point after which the Raman $5d$ yield decays.

The charge transfer times in Fig. 7 are obtained from the Raman yields of the $5d$ -state and the Auger channel. At 4788-eV x-ray excitation energy, the charge transfer time is 80 ± 1 as for [Au-Xe], 125 ± 1 as for [Cu-Xe], and 161 ± 1 as for [Ag-Xe]. All systems approach a value of tens of attoseconds for high excitation energies in the vicinity of 4793-eV photon energy. A value of 50 as falls within a common time-frame for excitations from deep core-holes in the tender x-ray regime and has been observed for K-edge excitation, e.g., silicon in SiO_2 (50 as) [53], phosphorous in InP (40 as) [54], sulfur in condensed $\text{C}_3\text{H}_7\text{SH}$ (100 as) [55] with processes observed in the KLL Auger region. These values are calculated by us using the data from the references and, apart from InP, using tabulated lifetime widths from Campbell *et al.* [52].

IV. SUMMARY

We have investigated Xe monolayers adsorbed on Cu, Ag, and Au substrates using hard x ray photoelectron spectroscopy. The thickness is determined from known chemical shifts of the Xe monolayers on Cu and Au. The x-ray absorption spectrum in the region of $[2p_{3/2}^{-1}] \rightarrow nd$ $n \geq 5$ has been studied via the structures in the electron energy distribution in the region of the Xe $L_3M_{4,5}M_{4,5}$ Auger electron kinetic energy region. By doing so, we can differentiate between contributions from coherent and incoherent decay channels

of the core excited state that build up the x-ray absorption cross section. Additionally, we can also determine the charge transfer time of core-excited states where the excited electron can tunnel away from the site of the excitation—states not available in the gas phase case. Using the core-hole clock method we find that the charge transfer time at threshold is 80 as for Au, 161 as for Ag, and 125 as for Cu with decreasing times approaching 50 as for all systems—a time frame which we find for KLL transitions of third row elements examining literature data. This is observed here in the LMM Auger decay channel.

In the 2D maps of the decay spectra, we observe two main channels for both substrates: one dispersive, interpreted as a coherent excitation of electrons into the $5d$ orbital from Xe $2p_{3/2}$ core level and a channel that occurs at constant kinetic energy, emanating from decays where the core-excited electron has tunneled away from the site hosting the core-hole—a state that decays in an Auger-like fashion. For the Au substrate, the two described channels dominate the spectral map together with an almost vanishing contribution from $nd > 5$ levels. The Cu and Ag substrates share all the mentioned features except that an extra resonating line is present for excitations between 4785 and 4791-eV x-ray energies, e.g., between the Fermi level of the system and the vacuum level. Theory indicates that electrons transferred to the substrate have a varying probability of remaining close to the core-excited atom providing screening of the core-hole, and this we observe experimentally as the extra intensity mentioned above at the high kinetic energy side of the normal Auger. This extra feature's intensity is substrate-dependent, and governed by the ground state hybridization. Ag and Cu exhibit negligible ground state charge transfer whereas Au change electron density in our model. This difference for the substrate-Xe interaction manifests itself in the calculation of doubly ionized Auger states (what we experimentally denote charge-transfer states) as parts of the Ag and Cu decay channels being shifted towards higher kinetic energies. Those channels are shifted by 1 to 2 eV below those of Ag, Cu for Au which means spectroscopically that those features coincide with the main feature and are thus not resolved.

Comparing to the gas phase a striking difference is the weakness of postcollision interaction process in the condensed phase. We attribute this to the complete screening by the substrate of the final state. Also, slow electrons with kinetic energies below the work function of the system cannot escape the sample—the same slow electrons that would contribute the largest PCI shifts in the gas phase (or free Xe cluster) system.

In conclusion we have investigated Xe monolayers on three metallic substrates using core-hole clock spectroscopy and compared those results with theory and literature data on gas phase Xe studied with the same methods. We demonstrate that ground state hybridization plays a crucial role in interpreting charge transfer dynamics in adsorbed systems and should encourage extension of these studies onto other condensed systems with varying properties. The resonant Auger spectroscopic technique allows the identification of the partial yields that build up the x-ray absorption cross-section—even a seemingly featureless x-ray absorption spectrum can be built up from a rich variety of parts.

ACKNOWLEDGMENTS

F.O.L.J acknowledges the support from the Swedish Research Council (Grant No. 2020-06409) A.L. acknowledges the support from the Swedish Research Council (Grant No. 2014-6463 and 2018-05336) and Marie Skłodowska Curie Actions (Cofund, Project INCA 600398). The research leading to this result has been supported by the project CALIPSOplus under the Grant Agreement No. 730872 from the EU Framework Programme for Research and Innova-

tion HORIZON 2020. We acknowledge synchrotron SOLEIL for the allocation of beamtime at the GALAXIES beamline through proposals No. 201902888 and 20200749. L.M.C. and H.Å. acknowledge the resources provided by the Swedish National Infrastructure for Computing (SNIC 2022-3-34) at the National Supercomputer Centre of Linköping University (Sweden) partially funded by the Swedish Research Council through Grant Agreement No. 2018-05973. L.M.C. also acknowledges Fundação de Amparo à Pesquisa do Estado de São Paulo (FAPESP) under Grant No. 2021/06527-7.

- [1] P. Le Fèvre, H. Magnan, D. Chandresris, J. Jupille, S. Bourgeois, W. Drube, H. Ogasawara, T. Uozumi, and A. Kotani, Interpretation of absorption edges by resonant electronic spectroscopy: Experiment and theory, *J. Electron Spectrosc. Relat. Phenom.* **136**, 37 (2004).
- [2] P. Heimann, D. Lindle, T. Ferrett, S. Liu, L. Medhurst, M. Piancastelli, D. Shirley, U. Becker, H. Kerkhoff, B. Langer *et al.*, Shake-off on inner-shell resonances of Ar, Kr and Xe, *J. Phys. B* **20**, 5005 (1987).
- [3] S. Svensson, B. Eriksson, N. Mårtensson, G. Wendin, and U. Gelius, Electron shake-up and correlation satellites and continuum shake-off distributions in x-ray photoelectron spectra of the rare gas atoms, *J. Electron Spectrosc. Relat. Phenom.* **47**, 327 (1988).
- [4] U. Becker, D. Szostak, M. Kupsch, H. G. Kerkhoff, B. Langer, and R. Wehlitz, Decay of the Xe 4d to np excitations: resonant shake-off versus shake-up and spectator transitions, *J. Phys. B: At., Mol. Opt. Phys.* **22**, 749 (1989).
- [5] U. Becker and D. Shirley, Threshold behaviour and resonances in the photoionization of atoms and molecules, *Phys. Scr.* **T31**, 56 (1990).
- [6] W. Wurth, Resonant Auger Raman effect for adsorbates, *Appl. Phys. A* **65**, 155 (1997).
- [7] C. Keller, M. Stichler, G. Comelli, F. Esch, S. Lizzit, D. Menzel, and W. Wurth, Resonant auger processes in adsorbates, *J. Electron Spectrosc. Relat. Phenom.* **93**, 135 (1998).
- [8] L.-Å. Näslund, M.-H. Mikkela, E. Kokkonen, and M. Magnuson, Chemical bonding of termination species in 2D carbides investigated through valence band UPS/XPS of $Ti_3C_2T_x$ MXene, *2D Mater.* **8**, 045026 (2021).
- [9] P. M. Korusenko, A. V. Koroleva, A. A. Vereshchagin, D. V. Sivkov, O. V. Petrova, O. V. Levin, and A. S. Vinogradov, The valence band structure of the [Ni (Salen)] complex: An ultraviolet, soft x-ray and resonant photoemission spectroscopy study, *Inte. J. Molecular Sci.* **23**, 6207 (2022).
- [10] R. K. Kushawaha, K. Jänkälä, T. Marchenko, G. Goldsztejn, R. Guillemin, L. Journel, D. Céolin, J. P. Rueff, A. F. Lago, R. Püttner, M. N. Piancastelli, and M. Simon, Auger resonant-Raman decay after Xe L-edge photoexcitation, *Phys. Rev. A* **92**, 013427 (2015).
- [11] T. Watanabe, Measurement of the L Absorption Spectra of Xenon, *Phys. Rev.* **137**, A1380 (1965).
- [12] C. Dezarnaud, F. Guillot, and M. Tronc, Near L-edge (4.7-5.5 Kev) photoionization in xenon, *J. Phys. B: At., Mol. Opt. Phys.* **25**, L123 (1992).
- [13] M. Žitnik, M. Kavčič, K. Bučar, A. Mihelič, M. Štuhec, J. Kokalj, and J. Szlachetko, Inelastic x-ray scattering in the vicinity of xenon L_3 edge, *Phys. Rev. A* **76**, 032506 (2007).
- [14] G. B. Armen, S. H. Southworth, J. C. Levin, U. Arp, T. LeBrun, and M. A. MacDonald, Xenon spectator and diagram $L_3-M_{4,5}M_{4,5}$ auger intensities near the L_3 threshold, *Phys. Rev. A* **56**, R1079 (1997).
- [15] G. S. Brown, M. H. Chen, B. Crasemann, and G. E. Ice, Observation of the Auger Resonant Raman Effect, *Phys. Rev. Lett.* **45**, 1937 (1980).
- [16] O. Karis, A. Nilsson, M. Weinelt, T. Wiell, C. Puglia, N. Wassdahl, N. Mårtensson, M. Samant, and J. Stöhr, One-Step and Two-Step Description of Deexcitation Processes in Weakly Interacting Systems, *Phys. Rev. Lett.* **76**, 1380 (1996).
- [17] N. Mårtensson, M. Weinelt, O. Karis, M. Magnuson, N. Wassdahl, A. Nilsson, J. Stöhr, and M. Samant, Coherent and incoherent processes in resonant photoemission., *App. Phys. A: Materials Science & Processing* **65**, 159 (1997).
- [18] P. Van der Straten, R. Morgenstern, and A. Niehaus, Angular dependent post-collision interaction in Auger processes, *Z. Phys. D: Atoms, Molecules Clusters* **8**, 35 (1988).
- [19] A. Lindblad, R. Fink, O. Björneholm, H. Bergersen, M. Lundwall, T. Rander, R. Feifel, G. Öhrwall, M. Tchapyguine, U. Hergenhahn *et al.*, Postcollision interaction in noble gas clusters: observation of differences in surface and bulk line shapes, *J. Chem. Phys.* **123**, 211101 (2005).
- [20] D. Céolin, J. Ablett, D. Prieur, T. Moreno, J.-P. Rueff, T. Marchenko, L. Journel, R. Guillemin, B. Pilette, T. Marin *et al.*, Hard x-ray photoelectron spectroscopy on the galaxies beamline at the soleil synchrotron, *J. Electron Spectrosc. Relat. Phenom.* **190**, 188 (2013).
- [21] M. Patanen, S. Aksela, S. Urpelainen, T. Kantia, S. Heinäsmäki, and H. Aksela, Free atom 4f photoelectron spectra of Au, Pb, and Bi, *J. Electron Spectrosc. Relat. Phenom.* **183**, 59 (2011), electron Spectroscopy Kai Siegbahn Memorial Volume.
- [22] E. Kukkk, G. Snell, J. D. Bozek, W.-T. Cheng, and N. Berrah, Vibrational structure and partial rates of resonant auger decay of the N 1s \rightarrow 2 π core excitations in nitric oxide, *Phys. Rev. A* **63**, 062702 (2001).
- [23] E. Kukkk, K. Ueda, U. Hergenhahn, X.-J. Liu, G. Prümper, H. Yoshida, Y. Tamenori, C. Makochekanwa, T. Tanaka, M. Kitajima *et al.*, Violation of the Franck-Condon Principle due to Recoil Effects in High Energy Molecular Core-Level Photoionization, *Phys. Rev. Lett.* **95**, 133001 (2005).
- [24] M. N. Piancastelli, G. Goldsztejn, T. Marchenko, R. Guillemin, R. K. Kushawaha, L. Journel, S. Carniato, J.-P. Rueff, D. Céolin,

- and M. Simon, Core-hole-clock spectroscopies in the tender x-ray domain, *J. Phys. B: At., Mol. Opt. Phys.* **47**, 124031 (2014).
- [25] L. Xin-Ying and C. Xue, *Ab initio* study of MXe_n^+ ($M = \text{Cu}, \text{Ag}, \text{and Au}; n = 1, 2$), *Phys. Rev. A* **77**, 022508 (2008).
- [26] I. Fdez. Galvan, M. Vacher, A. Alavi, C. Angeli, F. Aquilante, J. Autschbach, J. J. Bao, S. I. Bokarev, N. A. Bogdanov, R. K. Carlson *et al.*, Openmolcas: From source code to insight, *J. Chem. Theory Comput.* **15**, 5925 (2019).
- [27] M. Breinig, M. H. Chen, G. E. Ice, F. Parente, B. Crasemann, and G. S. Brown, Atomic inner-shell level energies determined by absorption spectrometry with synchrotron radiation, *Phys. Rev. A* **22**, 520 (1980).
- [28] K. Siegbahn, C. Nordling, G. Johansson, J. Hedman, P. Hedén, K. Hamrin, U. Gelius, T. Bergmark, L. Werme, R. Manne *et al.*, *ESCA: Applied to Free Molecules* (North-Holland Publishing Company, 1969).
- [29] B. E. Nieuwenhuys, R. Bouwman, and W. M. Sachtler, The changes in work function of group Ib and VIII metals on xenon adsorption, determined by field electron and photoelectron emission, *Thin Solid Films* **21**, 51 (1974).
- [30] A. Bendounan, Adsorption properties of Xe on Ag/Cu(111) system: Real-time photoemission investigation, *J. Phys. Chem. C* **120**, 24279 (2016).
- [31] J. Jupille, J.-J. Ehrhardt, D. Fargues, and A. Cassuto, Study of xenon layers on a Cu(111) surface, *Faraday Discuss. Chem. Soc.* **89**, 323 (1990).
- [32] J. Unguris, L. Bruch, E. Moog, and M. Webb, Xe adsorption on Ag(111): Experiment, *Surf. Sci.* **87**, 415 (1979).
- [33] D. P. Engelhart, R. J. Wagner, A. Meling, A. M. Wodtke, and T. Schäfer, Temperature programmed desorption of weakly bound adsorbates on Au(111), *Surf. Sci.* **650**, 11 (2016).
- [34] M. Kavčič, M. Žitnik, K. Bučar, A. Mihelič, B. Marolt, J. Szlachetko, P. Glatzel, and K. Kvashnina, Hard x-ray absorption spectroscopy for pulsed sources, *Phys. Rev. B* **87**, 075106 (2013).
- [35] A. G. Borisov, V. Sametoglu, A. Winkelmann, A. Kubo, N. Pontius, J. Zhao, V. M. Silkin, J. P. Gauyacq, E. V. Chulkov, P. M. Echenique *et al.*, π Resonance of Chemisorbed Alkali Atoms on Noble Metals, *Phys. Rev. Lett.* **101**, 266801 (2008).
- [36] J. Thomas, C. Bertram, J. Daru, J. Patwari, I. Langguth, P. Zhou, D. Marx, K. Morgenstern, and U. Bovensiepen, Competition between Coulomb and van der Waals Interactions in Xe-Cs⁺ Aggregates on Cu(111) Surfaces, *Phys. Rev. Lett.* **127**, 266802 (2021).
- [37] M. Weinelt, A. Nilsson, M. Magnuson, T. Wiell, N. Wassdahl, O. Karis, A. Föhlisch, N. Mårtensson, J. Stöhr, and M. Samant, Resonant Photoemission at the $2p$ Edges of Ni: Resonant Raman and Interference Effects, *Phys. Rev. Lett.* **78**, 967 (1997).
- [38] A. Föhlisch, O. Karis, M. Weinelt, J. Hasselström, A. Nilsson, and N. Mårtensson, Auger Resonant Raman Scattering in Itinerant Electron Systems: Continuum Excitation in Cu, *Phys. Rev. Lett.* **88**, 027601 (2001).
- [39] S. Tougaard, Quantitative analysis of the inelastic background in surface electron spectroscopy, *Surf. Interface Anal.* **11**, 453 (1988).
- [40] A. Lindblad, H. Bergersen, W. Pokapanich, M. Tchapyguine, G. Öhrwall, and O. Björneholm, Charge delocalization dynamics of ammonia in different hydrogen bonding environments: free clusters and in liquid water solution, *Phys. Chem. Chem. Phys.* **11**, 1758 (2009).
- [41] M. Lundwall, R. Fink, M. Tchapyguine, A. Lindblad, G. Öhrwall, H. Bergersen, S. Peredkov, T. Rander, S. Svensson, and O. Björneholm, Shell-dependent core-level chemical shifts observed in free xenon clusters, *J. Phys. B: At., Mol. Opt. Phys.* **39**, 5225 (2006).
- [42] A. Sandell, P. Brühwiler, A. Nilsson, P. Bennich, P. Rudolf, and N. Mårtensson, Nature of the ns-derived states for an isolated alkali atom on a surface, *Surf. Sci.* **429**, 309 (1999).
- [43] J. P. Gauyacq and A. G. Borisov, Excited electron transfer between a core-excited $\text{Ar}^*(2p_{3/2}^{-1}4s)$ atom and the metal substrate in the Ar/Cu(111) system, *Phys. Rev. B* **69**, 235408 (2004).
- [44] K. Wandelt, W. Jacob, N. d. Memmel, and V. Dose, Inverse Photoemission of Adsorbed Xenon Multilayers on Ru(001): Refutation of Final-State Screening Effects, *Phys. Rev. Lett.* **57**, 1643 (1986).
- [45] R. H. Temperton, S. T. Skowron, A. Gibson, K. Handrup, and J. N. O'Shea, Ultra-fast charge transfer between fullerenes and a gold surface, as prepared by electrospray deposition, *Chem. Phys. Lett.* **747**, 137309 (2020).
- [46] J. Tulkki, G. B. Armen, T. Åberg, B. Crasemann, and M. H. Chen, Quantum theory of post-collision interaction in inner-shell photoionization, *Z. Phys. D: Atoms, Molecules Clusters* **5**, 241 (1987).
- [47] G. B. Armen, J. Tulkki, T. Åberg, and B. Crasemann, Quantum theory of post-collision interaction in inner-shell photoionization: Final-state interaction between two continuum electrons, *Phys. Rev. A* **36**, 5606 (1987).
- [48] J. Tulkki, T. Åberg, S. B. Whitfield, and B. Crasemann, Quantum approach to photoelectron recapture in post-collision interaction, *Phys. Rev. A* **41**, 181 (1990).
- [49] S. Peters, S. Peredkov, B. Balkaya, N. Ferretti, M. Neeb, and W. Eberhardt, Evolution of metallic screening in small metal clusters probed by PCI–Auger spectroscopy, *Phys. Chem. Chem. Phys.* **12**, 9867 (2010).
- [50] F. Gel'mukhanov and H. Ågren, Resonant x-ray raman scattering, *Phys. Rep.* **312**, 87 (1999).
- [51] M. H. Chen, B. Crasemann, and H. Mark, Widths and fluorescence yields of atomic L-shell vacancy states, *Phys. Rev. A* **24**, 177 (1981).
- [52] J. Campbell and T. Papp, Widths of the atomic K–N7 levels, *At. Data Nucl. Data Tables* **77**, 1 (2001).
- [53] Y. Baba, H. Yamamoto, and T. Sasaki, KLL resonant Auger electron emission from silicon compounds in solid phase, *Surf. Sci.* **307-309**, 896 (1994).
- [54] H. Wang, J. C. Woicik, T. Åberg, M. H. Chen, A. Herrera-Gomez, T. Kendelewicz, A. Mäntykenttä, K. E. Miyano, S. Southworth, and B. Crasemann, Threshold KLL Auger spectra of P in InP, *Phys. Rev. A* **50**, 1359 (1994).
- [55] K. Yoshii, Y. Baba, and T. Sasaki, Resonant Auger electron spectra at Si-, P-, S-, and Cl-1s thresholds of condensed molecules, *Phys. Status Solidi (B)* **206**, 811 (1998).